M. Wirtz et al.

Influence of Helium Induced Nanostructures on the Thermal Shock Performance of Tungsten

17th International Conference on Fusion Reactor Materials (ICFRM), Aachen, Germany
(11th October 2015 – 16th October 2015)

Influence of Helium Induced Nanostructures on the Thermal Shock Performance of Tungsten

M. Wirtz, M. Berger, A. Huber, A. Kreter, J. Linke, G. Pintsuk, M. Rasinski, G. Sergienko, B.Unterberg

Forschungszentrum Jülich GmbH, Institut für Energie- und Klimaforschung, 52425 Jülich, Germany

* Corresponding author
Last name: Wirtz
First name   Marius
Address: Forschungszentrum Jülich
                IEK-2
                Wilhelm-Johnen-Straße
                52428 Jülich, Germany
e-mail: m.wirtz@fz-juelich.de
tel.:   + 49 2461 61 5843

Abstract

Experiments were performed in the linear plasma device PSI-2 in order to investigate the synergistic effects of combined steady-state He-plasma and thermal shock exposure. Tungsten produced according to the ITER material specifications by Plansee SE, Austria, was loaded sequentially and simultaneously by steady-state He plasma and transient thermal loads induced by a laser beam. All tungsten samples were exposed to helium plasma for 40 min at a base temperature of ca. 850 °C and a flux of ca. 2.8×10^{22} $m^{-2}s^{-1}$. Before, during and after the plasma exposure 1000 thermal shock pulses with a pulse duration of 1 ms and a power density 0.76 GW/m² were applied on the samples. The thermal shock exposure before and after plasma exposure was done at room temperature in order to investigate helium induced surface effects also within cracks. The obtained results show that the combination of He plasma with transient thermal shock events results in a severe modification such as reduced height or agglomeration of the sub-surface He-bubbles and of the created nanostructures, i.e. W-fuzz.

Keywords:
Tungsten, edge localized mode, transient thermal loads, W-fuzz, synergistic effects

Highlights

- Combined steady-state He-plasma and thermal shock exposure of W.
- Strong modification of the W-fuzz, if combined with thermal shocks.
- He induced nanostructures grow in cracks and enhance the risk of erosion.
- Formation of He-bubbles near the surface reduces the thermal conductivity.
- Alteration of laser absorption due to W-fuzz influences the thermal shock behavior.

1   Introduction

In future fusion devices such as ITER and DEMO plasma facing materials (PFMs) will be exposed to extreme and complex environmental conditions, especially in the divertor region. This comprises not only steady state and transient thermal loads like edge localized modes (ELMs), vertical displacement events (VDEs) and plasma disruptions but also high hydrogen, helium and neutron fluxes [1-3]. Especially the surface near implantation of helium leads, depending on the surface temperature, to significant material modifications such as the formation of helium bubbles within the implantation zone as well as the growth of columnar structures so-called tungsten fuzz on the surface [4,5]. The synergistic effects of a combined exposure of tungsten to particle fluxes and transient thermal loads have not been extensively studied yet.

Tungsten is the main candidate material for an application in the divertor region to withstand these severe conditions for an appropriate time before the components need to be replaced. However, earlier studies have shown that transient thermal loads induce a wide range of surface modifications such as roughening, small cracks and crack networks on the PFM surface [6,7]. For the assessment of tungsten as PFM it is crucial to know how the material will behave not only under pure thermal loads but also under combined particle and high heat load exposure.

Therefore, this work focusses on the successive and simultaneous exposure of tungsten samples to a steady-state He-plasma combined with transient thermal loads simulated by a laser beam. Especially the different loading sequences allow studying how the different kinds of loadings (heat and particle) interact with each other and what will be the possible consequences for the performance of tungsten in a tokamak like ITER or DEMO.

2   Experimental

The investigated material is a tungsten grade with a purity of 99.97 wt% provided by Plansee SE, Austria. It was manufactured according to the ITER material specifications [8] using and a subsequent stress relieving treatment by thermal annealing. Due to the production process the grain structure is strongly elongated with needle like grains parallel to the forging direction. Samples with the dimension $12 \times 12 \times 5$ mm³ were cut from the tungsten rod with a transversal grain orientation (grains elongated perpendicular to the loaded surface). All samples were mechanically polished to a mirror finish to obtain an undamaged well-defined reference state.

The experiments with successive and simultaneous exposure to He-plasma and transient heat loads were done in the linear plasma device PSI-2 [9] similar to the procedure describe in [10]. An actively cooled copper block connected via ceramic bar spacers with the sample holder, comprising an integrated ohmic heating plate, was used to achieve high base temperatures of the sample. The sample was fixed with a tungsten mask (exposure window 10×12 mm²) in the region with the maximum plasma flux density. The reflection/transmission of each part of the optical system was measured by a photo diode in order to determine the absorbed power density. Furthermore, the reflectance of the polished sample surface at $\lambda = 1064$ nm is 60 % [10] and the temperature dependence of the emissivity at $\lambda = 1064$ nm is negligible according to [11]. The successive and simultaneous exposure was performed in three different steps.

Step A: A Nd:YAG laser ($\lambda = 1064$ nm) with an maximum energy of 32 J was used to simulated ELM like transient heat loads. The tests were performed with an absorbed power density of 0.76 GW/m² (for a polished surface, surface temperature rise ~1400 °C) and the base temperature set to room temperature (RT). A circular area with a diameter of 3 mm was exposed to 1000 pulses with a repetition frequency of 0.5 Hz and a pulse duration of 1 ms.

Step B: The parameters during the He-plasma exposure were a source current of 250 A, a plasma flux of $2.8 \times 10^{22} \, m^{-2}s^{-1}$ and a particle energy of ~52 eV (biasing of 80 V). The tungsten target (area $10 \times 12 \, mm^2$) was exposed to plasma until the sample temperature reached steady state conditions of 850 °C measured by a thermocouple. After achieving constant plasma and surface temperature conditions the laser exposure was started at the second position with the same conditions as in step A. Based on the number of thermal shock pulses the He-ion fluence was $5.5 \times 10^{25} \, m^{-2}$.

Step C: After the simultaneous exposure (step B) the plasma was switched off and the laser beam was moved to the last position. 1000 laser pulses were applied with the same parameters as in step A and B after the sample cooled down to RT.

This stepwise exposure, similar to the procedure in [10], of the tungsten target in PSI-2 results in four different loading sequences: laser followed by plasma exposure (step A), simultaneous laser and plasma exposure (step B), plasma followed by laser exposure (step C) and as reference the remaining surface area only exposed to plasma.

After the exposure in PSI-2 the induced damages and surface modifications were analyzed by scanning electron microscopy (SEM) and focused ion beam (FIB) cross sections.

3　　　Results and Discussion

The successful generation of He induced nanostructures (fuzz) on tungsten under the in section 2 described conditions is depicted in figure 1. The SEM images show the only He-plasma exposed tungsten surface at different magnifications (Figure 1a and b) and a FIB-cross section (Figure 1c). A very uniform and smooth W-fuzz layer with a thickness of 2.06 ± 0.18 μm was created, which consists of fine tungsten filaments with a diameter of several nanometers. The thickness was measured on the basis of the cross section in Figure 1c and therefore the statistics is very low but due to the homogeneity shown in figure 1a and b the value is regarded as representative. Furthermore, nanometric He-bubbles are formed several μm below the loaded surface, which will reduce the thermal conductivity in the surface near region [12].
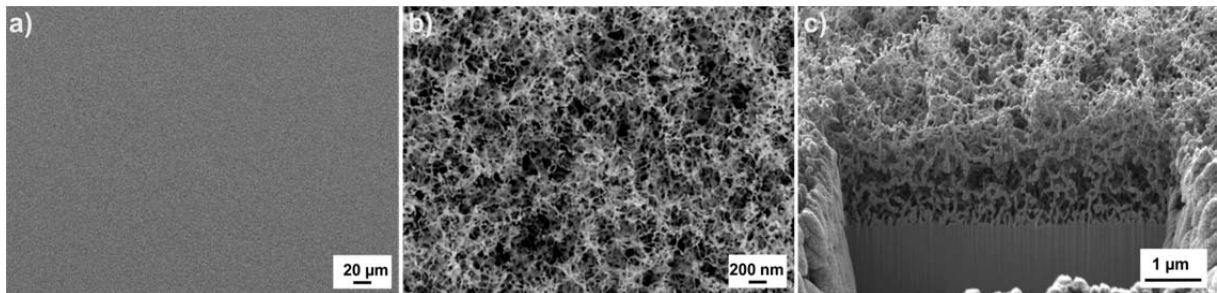

Figure 1: SEM images of the only He-plasma exposed tungsten surface. 1a and b show the loaded surface at different magnifications. 1c shows a FIB-cross section of the W-fuzz and the material below.

Figure 2 shows SEM images of the loaded surfaces after the sequential or simultaneous exposure to steady-state He-plasma and transient thermal loads. The comparison with the only He-plasma exposed surface (Figure 1) illustrates clearly that the combined exposure with transient thermal loads has a significant influence on the formation of the He induced nanostructures. Furthermore, the sequence of these exposure conditions has also a strong impact on the occurring surface modifications/damages.

The thermal shock exposure at RT induced thermal shock crack networks on the loaded surfaces (Figure 2a, d, c, f) as it was also reported in earlier studies with pure thermal loading [13,14] independent from the pre-/post-exposure to He-Plasma. However, the He-plasma exposure of a cracked surface shows that the W-fuzz does not only grow on the sample

surface but also at the crack edges and even at the surfaces insides the crack itself (Figure 2d and 3a). In contrast to that no W-fuzz was found inside the cracks if the He-Plasma exposure was done before the thermal shock loading (Figure 2c, f).

Another major difference between the two sequential loading conditions is the W-fuzz formation/appearance in the non-cracked parts of the sample surface. The comparison of Figure 2a with the only He-plasma exposed reference (Figure 1) shows that the W-fuzz surface with the thermal shock pre-loading is not as smooth as the reference one. A possible explanation for this is that the thermal shock events induce surface modifications/roughening due to plastic deformation. However, the He-fuzz itself appears very similar to the reference state.

In contrast to that the post-exposure of the W-fuzz to thermal shock events shows a significant modification of the surface structures (Figure 2c, f). Besides the severe roughening of the loaded surface, the fine filament structure of the He-fuzz almost disappeared. There are only occasional distributed agglutinated W-fuzz like filaments left and also small droplets of molten materials can be found on the surface.
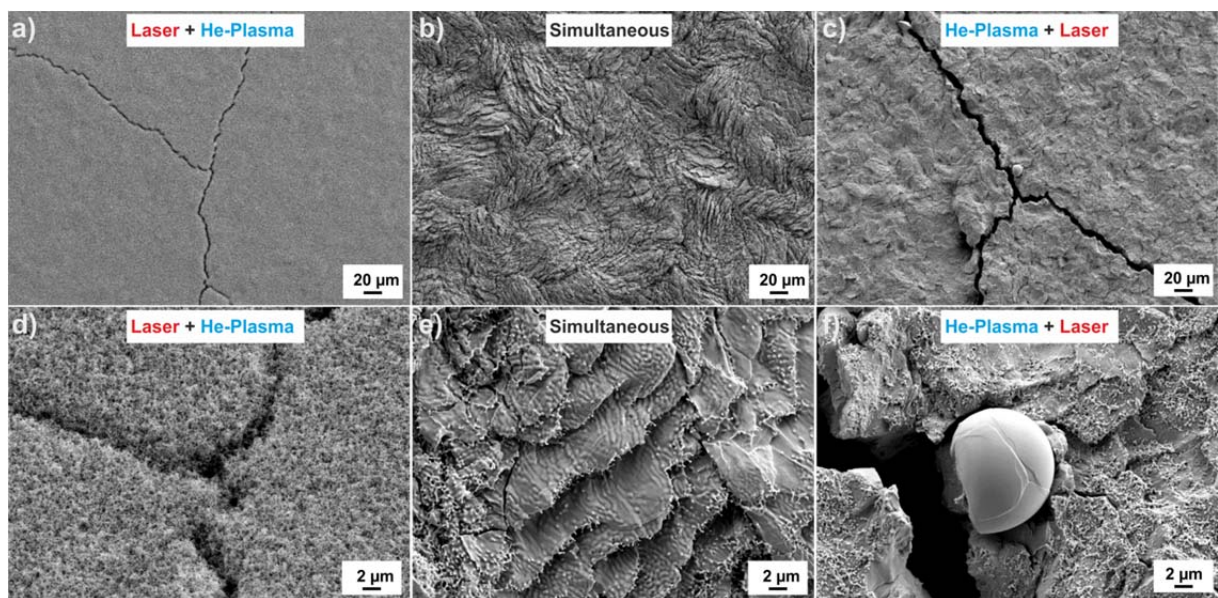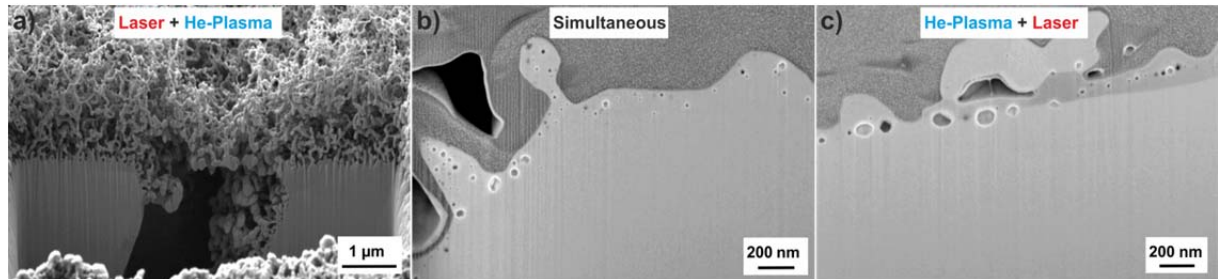

Figure 2: SEM images the He-plasma and laser exposed surfaces (absorbed power density 0.76 GW/m², 1000 pulses): a) and d) first laser at RT than He-plasma exposure at 850 °C; b) and e) simultaneous laser and He-plasma exposure at 850 °C; c) and f) first He-plasma at 850 °C than laser exposure at RT.

For the simultaneous exposure of the tungsten target to steady-state He-plasma and thermal shocks the base temperature was also for the thermal shock loading at 850 °C, which is in contrast to the sequential experiments. At this high base temperature tungsten is in a ductile state and therefore no brittle thermal shock crack networks were found on the loaded surface (Figure 2b and e). Nevertheless, strongly pronounced surface modifications such as roughening due to plastic deformation were induced. Scale like structures are formed on the whole laser exposed surface which are covered with W-fuzz like filaments similar to the structures observed on the He-plasma pre-exposed surface. This similarity is supported by the FIB-cross section in Figure 3b and c.

Beside the surface modification and crack networks the FIB-cross sections (Figure 3) depict that He-bubbles in the nanometer ranged are formed directly below the surface for all three loading sequences. These bubbles are also visible on the surface itself for the simultaneous exposure where they form small holes/pores, which are distributed over the laser exposed surface. On the basis of these cross sections also the height/thickness of the W-fuzz and the

He affected surface (thickness of the bubble layer) was measured. The W-fuzz formed after the thermal shock performance has a comparable height to the only He-plasma exposed reference one in the range of $1.98 \pm 0.08\,\mu m$. In contrast to that the thickness of the agglutinated W-fuzz like filaments and the He-bubble layer is $0.61 \pm 0.05\,\mu m$ and $0.35 \pm 0.13\,\mu m$ for the simultaneous and the He-plasma pre-exposed spot, respectively. As mentioned before, the errors of these measurements are quite large because of the difficulty to define the end of the He-affected zone and the low statistics. Nevertheless, the values are very useful for a qualitative comparison among the different loading sequences.

Figure 3: FIB-cross section the He and laser exposed surfaces (absorbed power density 0.76 GW/m², 1000 pulses): a) first laser at RT than He-plasma exposure at 850 °C; b) simultaneous laser and He-plasma exposure at 850 °C; c) first He-plasma at 850 °C than laser exposure at RT. The dark gray parts in b) and c) are attributed to the protective metallic layer co-deposited before the cutting.

Explanations for the severe modifications of the W-fuzz, especially for the simultaneous and He-plasma pre-exposed loading, could be melting of the He induced nanostructure or outgassing of the He bubbles combined with an viscoelastic flow back to the surface. Although the surface temperature rise during the thermal shock event is around 1400 °C for a pristine surface the W-fuzz changes the optical properties of the surface which results in a laser light ($\lambda = 1064\,nm$) absorption of nearly 100 %. Due to that the absorbed power density would be 1.5 GW/m² and this corresponds to an increase of the surface temperature of ~2800 °C. Cooperatively with the base temperature of 850 °C for the simultaneous exposure this could lead to melting of a near surface layer and would explain the small waves on the scale structures in Figure 2e. In contrast to that these waves are not visible on the He-plasma pre-exposed surface (Figure 2f) where the sample was at RT during the thermal shock exposure. Here the annealing/viscoelastic flow back to the surface could be the major reason for the strong modification of the W-fuzz. Additionally, the formation of W-fuzz and He-bubbles below the surface reduces the thermal conductivity in the near surface region and therefore also leads to an increase of the surface temperature during the thermal shock event [12].

The formation of W-fuzz inside thermal shock induced cracks and the crack bridging by the W-fuzz (figure 3a), which was also observed in earlier experiments at GLADIS and JUDITH 1 [15], increases the risk of erosion and dust formation. During a thermal shock the crack width will become smaller or it even closes completely due to the thermal expansion of the material which will apply compressive forces and probably frictional loads on this crack filling structures. The mechanical strength and stability of these structures are not yet known and further investigations are needed for clarification of this issue.

Scale like structures (Figure 2e) were also observed after combined deuterium and thermal shock exposure experiments on tungsten [10,16] but the reasons and mechanisms for the formation of such structures are not finally clarified. The up to now obtained results indicate that the microstructure has an influence on the formation of these surface phenomena. Due to the loose contact to the underlying material and the therefore reduced thermal

conductivity/heat dissipation the scale like structures could overheat and melt during further thermal shock exposure.

4 Summary & Conclusions

Based on the above presented results it can be stated that the combined exposure of steady-state He-plasma and transient thermal loads has a significant influence on the formation of He-induced nanostructures on tungsten surfaces. The induced surface modifications range from roughening due to plastic deformation, thermal shock crack networks and the formation of small cracks in the micrometer range. These types of damage do not vary a lot from the ones induced by pure thermal exposure [13]. However, a closer analysis of the exposed surface and the interaction of He particle exposure with the thermal shock events shows that there are significant differences which may have an impact on the performance of tungsten as PFM in a fusion reactor environment.

Especially the formation of W-fuzz within cracks and the bridging of these cracks could lead to enhanced erosion and formation of dust. The formation of He-bubbles in a near surface region will have an influence on the thermal conductivity and the heat dissipation. This could cause overheating and melting of the PFM surface particular in areas where the heat dissipation is already reduced, e.g. for the scale like structures or for surface after very high pulse numbers [17]. Additionally, the mechanical properties will change due to the He implantation what will also have a significant influence on the thermal shock resistance of tungsten [12].

Further experiments are planned in order to understand the underlying mechanisms which are responsible for the significant changes of the W-fuzz morphology due to the combined thermal shock exposure. So-called damage mappings are planned with varying power densities, base temperatures and plasma parameters as well as higher pulse numbers in the range of 10^6, amongst others to create thermal fatigue induced crack networks on the surface. This will help to quantify the impact of these synergistic effects on the performance of tungsten as PFM.

5 Acknowledgment

6 References

[1] A. Loarte, G. Saibene, R. Sartori, V. Riccardo, P. Andrew, J. Paley, W. Fundamenski, T. Eich, A. Herrmann, G. Pautasso, A. Kirk, G. Counsell, G. Federici, G. Strohmayer, D. Whyte, A. Leonard, R. A. Pitts, I. Landman, B. Bazylev, S. Pestchanyi. Physica Scripta, 2007 (2007) 222-228

[2] R.A. Pitts, S. Carpentier, F. Escourbiac, T. Hirai, V. Komarov, S. Lisgo, A.S. Kukushkin, A. Loarte, M. Merola, A. Sashala Naik, R. Mitteau, M. Sugihara, B. Bazylev, P.C. Stangeby. Journal of Nuclear Materials 428 (2013) S48-S56

[3] Y. Ueda, J. W. Coenen, G. De Temmerman, R. P. Doerner, J. Linke, V. Philipps, E. Tsitrone. Fusion Engineering and Design 89 (2014) 901-906

[4] Shuichi Takamura, Noriyasu Ohno, Dai Nishijima, Shin Kajita. Plasma and Fusion Research: Rapid Communications 1 (2006) 051-1-051-2

[5] S. Kajita, W. Sakaguchi, N. Ohno, N. Yoshida, T. Saeki. Nuclear Fusion 49 (2009) 095005

[6] G. Pintsuk, A. Prokhodtseva, I. Uytdenhouwen. Journal of Nuclear Materials 417 (2011) 481-486

[7] M. Wirtz, J. Linke, G. Pintsuk, L. Singheiser, I. Uytdenhouwen. Physica Scripta T145 (2011) 014058

[8] ITER Materials Assessment Report (MAR), ITER Doc. G 74 MA 10 01-07-11 W0.3

[9] A. Kreter, C. Brandt, A. Huber, S. Kraus, S. Möller, M. Reinhart, B. Schweer, G. Sergienko, B. Unterberg. Fusion Sci. Technol. 68 (2015) 8–14

[10] M. Wirtz, S. Bardin, A. Huber, A. Kreter, J. Linke, T.W. Morgan, G. Pintsuk, M. Reinhart, G. Sergienko, I. Steudel, G. De Temmerman, B. Unterberg. Nuclear Fusion 55 (2015) 123017

[11] G.D. Rieck 1967 Tungsten and its Compounds 1st edn (Oxford: Pergamon)

[12] N. Yoshida, H. Iwakiri, K. Tokunaga, T. Baba. Journal of Nuclear Materials 337-339 (2005) 946-950

[13] M. Wirtz, J. Linke, Th. Loewenhoff, G. Pintsuk, I. Uytdenhouwen. Physica Scripta, in press

[14] M. Wirtz, J. Linke, G. Pintsuk, L. Singheiser, M. Zlobinski.Journal of Nuclear Materials 438 (2013) S833-S836

[15] N. Lemahieu, H. Greuner, J. Linke, H. Maier, G. Pintsuk, M. Wirtz, G. Van Oost, J.-M. Noterdaeme. Fusion Engineering and Design, submitted

[16] I. Steudel, A. Huber, A. Kreter, J. Linke, G. Sergienko, B. Unterberg, M. Wirtz. Physica Scripta, in press

[17] Th. Loewenhoff, J. Linke, G. Pintsuk, C. Thomser. Fusion Engineering and Design 87 (2012) 1201-1205